IET Generation, Transmission & Distribution

Research Article

IET Journals
The Institution of Engineering and Technology

Identification of modal interaction and small signal stability in autonomous microgrid operation

ISSN 1751-8687
Received on 2nd August 2017
Accepted on 4th August 2017
E-First on 13th November 2017
doi: 10.1049/iet-gtd.2017.1219
www.ietdl.org

Awan Uji Krismanto[1,2], Nadarajah Mithulananthan[1] ✉

[1]*School of ITEE, University of Queensland, Brisbane, Australia*
[2]*Department of Electrical Engineering, National Institute of Technology, Malang, Indonesia*
✉ *E-mail: mithulan@itee.uq.edu.au*

Abstract: The detailed models of renewable energy resources based distributed generation (DG) unit, namely, wind energy conversion system, photovoltaic and diesel engine are presented in this study. Combination of different DG units in three microgrid (MG) structures is considered to investigate small signal stability and possible interaction between sensitive modes, particularly in autonomous mode of MG operation. Evaluation of oscillatory condition suggested that gain controller variation significantly influenced MG stability and system dynamic response. Moreover, since modal interaction potentially occurred due to gain change, it is necessary to identify the interaction accurately to ensure stable MG operation. The conventional identification method of eigen-interaction is conducted by observing the movements of engaged eigenvalues. However, the eigen-trajectories method is less sensitive to identify the occurrence of weak interaction. To provide more sensitive identification method, cross-participation factor (CPF) and modal interaction index (MII) analysis are proposed. Deviation of eigen-trajectories after approaching a particular interaction point, higher values of CPF and MII confirmed the occurrence of interactions. The presented works contribute for MGs gain setting consideration and proposing novel methodologies in identifying modal interaction.

1 Introduction

Power generation based on renewable energy resources (RES) is expected to play a significant role in future electric grid due to its advantages in lowering carbon emission, reducing expansion cost and enhancing power quality [1]. However, uncertainties of RES have been a major concern to ensure stable operation and reliability of electricity supply of individual distributed generation (DG). Hence, it is necessary to combine a group of DG units into a single coordinated and controlled power system known as microgrid (MG). MG system allows seamless connection of more RES integration. Moreover, it enhances the power quality and continuity of electricity service for remote area customers.

Even though MG brings advantages for injecting additional power in the existing grid, it may introduce new challenges in particular during islanding operation. Small load change, feedback controller and a limited amount of DG units physical inertia potentially lead to instability concerns [2, 3]. In conventional power system with strong inertia features, gain variations do not introduce significant impact on equilibrium point and stability [4]. Conversely, MG with its less inertia characteristic is very susceptible to small perturbation on system parameter involving gain controller. Hence, it is necessary to provide a comprehensive study of oscillatory conditions in MG due to gain variations to ensure stable operation of MG [5–7]. Moreover, sophisticated MG control algorithm introduces more non-linear effect on modal behaviour which potentially leads to the occurrence of modal interaction [8]. The interaction may cause more oscillatory and indeed instability situations [4, 9, 10]. Hence, it is important to monitor the eigen-interactions to maintain the MG stability.

In this paper, a comprehensive MG model of three different configurations is investigated to provide a complete understanding of small signal stability performance and modal interaction. Commonly, eigen-trajectories monitoring was implemented to confirm the modal interaction [4, 9, 11]. However, the method is not sensitive to weak interaction. To enhance the previous identification process, two analytical procedures comprising of cross-participation factor (CPF) and modal interaction index (MII) methods are proposed. The remainder of this paper is organised as follows. MG structures and their controllers considered in this research are presented in Section 2. Section 3 describes procedures for small signal stability and modal interaction analysis. The simulation results and discussions of MG small signal stability and modal interaction are provided in Section 4. Conclusions and contributions of this paper are highlighted in Section 5.

2 MG model

Fig. 1 represents block diagrams of the investigated MG systems. Three MG structures comprising of wind energy conversion system (WECS), photovoltaic (PV) and diesel engine (DE) generator and their controllers are considered. Two-stage converters of DC/DC and DC/AC are implemented to form PV-based DG. While to provide full power conversion from available wind resource, fully rated WECS type incorporating back-to-back AC/DC/AC inverter is selected. DE is integrated to ensure power balance during shortfall power from wind and sun.

Since all DG units are operated in its individual reference frame, it is necessary to synchronise all of them into a common reference frame. Synchronisation of DGs is realised using transformation matrices of $\boldsymbol{T}_c$, $\boldsymbol{T}_{c\delta}$, $\boldsymbol{T}_v$ and $\boldsymbol{T}_{v\delta}$ from [3]. In this paper, DE is considered as common reference frame hence output state variables of PV, and WECS DGs have to be translated into DE reference frame. Uppercase and lowercase indices correspond to the positions of state variables in common and individual reference frames, respectively, while zero indices are associated with the initial condition of the state variables.

2.1 Line impedance and load model

The connection between DGs local and point of common coupling (PCC) bus are facilitated by distribution lines which can be modelled as a series RL impedance (R_{li} and L_{li}). State equations of lines currents ($i_{\mathrm{lik}D}$, $i_{\mathrm{lik}Q}$) is given by (see (1)) where $\boldsymbol{\Delta x}_{\mathrm{line}} = \left[\Delta i_{\mathrm{lik}D} \quad \Delta i_{\mathrm{lik}Q}\right]^{\mathrm{T}}$, $\boldsymbol{\Delta v}_{\mathrm{blinekDQ}} = \left[\Delta v_{bkD} \quad \Delta v_{bkQ}\right]^{\mathrm{T}}$, $\boldsymbol{\Delta v}_{\mathrm{pccDQ}} = \left[\Delta v_{\mathrm{pccD}} \quad \Delta v_{\mathrm{pccQ}}\right]^{\mathrm{T}}$

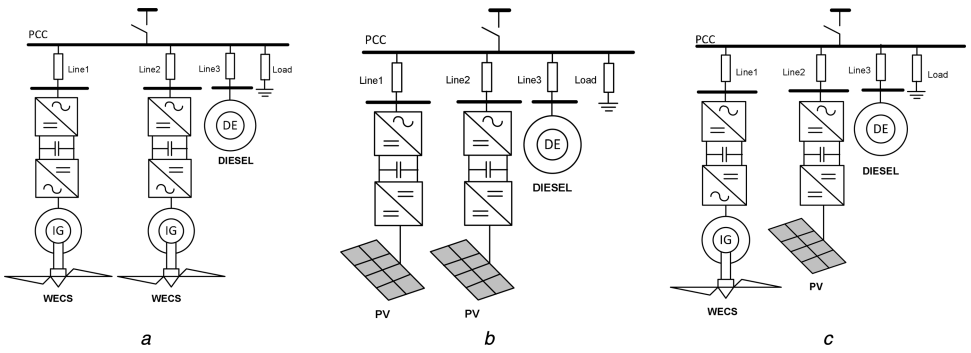

Fig. 1 *Configurations of investigated MG architectures*
(a) 2-WECS 1-DE MG, ***(b)*** 2-PV 1-DE MG, ***(c)*** Hybrid WECS PV DE MG

$$\boldsymbol{A}_{\text{linek}} = \begin{bmatrix} -R_{\text{lik}}/L_{\text{lik}} & -\omega_0 \\ \omega_0 & -R_{\text{lik}}/L_{\text{lik}} \end{bmatrix},\ \boldsymbol{B}_{\text{linek}} = \begin{bmatrix} 1/L_{\text{lik}} & 0 \\ 0 & 1/L_{\text{lik}} \end{bmatrix},$$
$$\boldsymbol{B}_{\text{linekpcc}} = \begin{bmatrix} -1/L_{\text{lik}} & 0 \\ 0 & -1/L_{\text{lik}} \end{bmatrix},\ \boldsymbol{B}_{\text{linekDE}} = \begin{bmatrix} I_{\text{lik0}Q} \\ -I_{\text{lik0}D} \end{bmatrix},\ k = 1, 2, 3$$

The load impedance (R_{lo} and L_{lo}) is considered to model a central load. State equation of the load currents ($i_{\text{lo}D}$, $i_{\text{lo}Q}$) is given by

$$\Delta\dot{\boldsymbol{x}}_{\text{lo}} = \boldsymbol{A}_{\text{lo}}\Delta\boldsymbol{x}_{\text{lo}} + \boldsymbol{B}_{\text{lo}}\Delta\boldsymbol{v}_{\text{pcc}DQ} + \boldsymbol{B}_{\text{lo}DE}\Delta\omega_{\text{ref}} \tag{2}$$

where

$$\Delta\boldsymbol{x}_{\text{lo}} = \begin{bmatrix} \Delta i_{\text{lo}D} & \Delta i_{\text{lo}Q} \end{bmatrix}^{\text{T}}, \boldsymbol{A}_{\text{lo}} = \begin{bmatrix} -R_{\text{lo}}/L_{\text{lo}} & \omega_0 \\ -\omega_0 & -R_{\text{lo}}/L_{\text{lo}} \end{bmatrix}, \boldsymbol{B}_{\text{lo}} = \begin{bmatrix} -1/L_{\text{lo}} & 0 \\ 0 & -1/L_{\text{lo}} \end{bmatrix},\ \boldsymbol{B}_{\text{lo}DE} = \begin{bmatrix} I_{\text{lo}Q} \\ -I_{\text{lo}D} \end{bmatrix}$$

The connection between state equations of lines, load currents and bus voltages are facilitated by applying a virtual resistance (R_N) in the corresponding buses. Hence, estimation of local and PCC bus voltages can be accurately determined as

$$\Delta\boldsymbol{v}_{bkDQ} = R_N\left[\Delta\boldsymbol{i}_{\text{o}kDQ}\right] - R_N\left[\Delta\boldsymbol{i}_{\text{lik}DQ}\right] \tag{3}$$

$$\Delta\boldsymbol{v}_{\text{pcc}DQ} = R_N\left[\Delta\boldsymbol{i}_{\text{lik}DQ}\right] - R_N\left[\Delta\boldsymbol{i}_{\text{lo}DQ}\right] \tag{4}$$

where $\boldsymbol{i}_{\text{o}kDQ}$ represents the output current of kth DG unit in D and Q reference frame.

2.2 Diesel engine generator model

A dynamic model of a synchronous generator in DE-based DG unit is presented in the form of a non-reduced order model involving dynamics at stator, rotor and damper winding. State variables of DE are represented by two q-axis (i_{kq1}, i_{kq2}) and one d-axis (i_{kd}) rotor currents, one d–q-axis ($i_{\text{s}d}$, $i_{\text{s}q}$) stator currents and excitation current (i_{fd}). Input variables are mechanical torque ($T_{\text{M}de}$), field winding voltage ($v_{\text{f}d}$) and stator side terminal voltage ($v_{\text{s}d}$, $v_{\text{s}q}$). It is assumed that stator voltage is similar to local bus voltage (v_{bD}, v_{bQ}). The state-space model is then completed with mechanical equations of the turbine and electromagnetic torque equation. DE is considered as a standard reference frame which is responsible for providing a reference for other DGs. Output variables of the DE are stator current ($i_{\text{s}D}$, $i_{\text{s}Q}$) and reference angular frequency (ω_{ref}). Development of detailed DE state-space model is derived from [12, 13]. Linearised state-space model of DE is given by

$$\Delta\dot{\boldsymbol{x}}_{\text{DE}} = \boldsymbol{A}_{\text{DE}}\Delta\boldsymbol{x}_{\text{DE}} + \boldsymbol{B}_{\text{DE}}\Delta\boldsymbol{u}_{\text{DE}} + \boldsymbol{B}_{v\text{DE}}\Delta\boldsymbol{v}_{b3}$$
$$\begin{bmatrix} \Delta i_{\text{s}D} \\ \Delta i_{\text{s}Q} \\ \Delta\omega_{\text{ref}} \end{bmatrix} = \begin{bmatrix} \boldsymbol{C}_{\text{DE}1} \\ \boldsymbol{C}_{\text{DE}2} \end{bmatrix}\Delta\boldsymbol{x}_{\text{DE}} \tag{5}$$

where

$$\Delta\boldsymbol{x}_{\text{DE}} = \begin{bmatrix} \Delta i_{sd} & \Delta i_{sq} & \Delta i_{fd} & \Delta i_{kd} & \Delta i_{kq1} & \Delta i_{kq2} & \Delta\omega_{\text{ref}} & \Delta\delta_{\text{DE}} \end{bmatrix}^{\text{T}},$$
$$\Delta\boldsymbol{u}_{\text{DE}} = \begin{bmatrix} \Delta v_{fd} & T_{\text{MDE}} \end{bmatrix}^{\text{T}},\ \Delta\boldsymbol{v}_{b3} = \begin{bmatrix} \Delta v_{b3d} & \Delta v_{b3q} \end{bmatrix}^{\text{T}}$$

$$\boldsymbol{B}_{v\text{DE}} = \begin{bmatrix} 1/L_{\text{li}3} & 0 \\ 0 & 1/L_{\text{li}3} \end{bmatrix}, \boldsymbol{C}_{\text{DE}1} = \begin{bmatrix} 1 & 0 & 0_{1\times 6} \\ 0 & 1 & 0_{1\times 6} \end{bmatrix},\ \boldsymbol{C}_{\text{DE}2} = \begin{bmatrix} 0_{1\times 6} & 1 & 0 \end{bmatrix}$$

Substitution of (3) into (5) represents the connection between this DG unit and line impedance. Hence, state equation of DE can be rewritten as

$$\Delta\dot{\boldsymbol{x}}_{\text{DE}} = (\boldsymbol{A}_{\text{DE}} + R_N\boldsymbol{B}_{v\text{DE}}\boldsymbol{C}_{\text{DE}1})\Delta\boldsymbol{x}_{\text{DE}} + \boldsymbol{B}_{\text{DE}}\Delta\boldsymbol{u}_{\text{DE}} + \boldsymbol{B}_{\text{DEline}}\Delta\boldsymbol{x}_{\text{line}} \tag{6}$$

where $\boldsymbol{B}_{\text{DEline}} = R_N\left[0_{8\times 4} \quad \boldsymbol{B}_{v\text{DE}}\right]$.

2.3 Two-stage PV model

Two-stage PV system mainly consists of PV array, DC/DC and DC/AC power converter. Regulation of fluctuated DC voltage from PV array is achieved by controlling the duty cycle of DC/DC converter. The regulated DC voltage is then fed to the DC/AC voltage source inverter (VSI) to generate a stable output power. Averaged model of DC/DC considering state variables of input current (i_b), output current (i_{s}), output DC/DC voltage (v_b) and DC link capacitor voltage (v_{dc}) are derived from [14]. A general mathematic model of DC/AC converter is derived from [15]. State variables of complete DC/AC inverter comprise of DC side current (i_{s}), DC side voltage (v_{dc}), VSI current ($i_{\text{i}d}$, $i_{\text{i}q}$), output current ($i_{\text{o}d}$, $i_{\text{o}q}$) and output voltage ($v_{\text{o}d}$, $v_{\text{o}q}$). Interface low-pass filter and coupling impedance are then attached to the system to mitigate high-frequency components.

In general, control algorithms in RES based DGs comprise of input and grid side power electronic devices controllers as depicted in Fig. 2. Proposed control scheme of input side DC/DC boost converter is responsible for ensuring a stable DC link voltage as shown in Fig. 2*a*. The reference voltage is compared with the measured DC link voltage and obtained error is then regulated by proportional–integral (PI) controller to generate duty cycle (d) control signal for DC/DC converter. State equation of input side controller is given by

$$\Delta\dot{\boldsymbol{x}}_{\text{line}} = \boldsymbol{A}_{\text{line}}\Delta\boldsymbol{x}_{\text{line}} + \boldsymbol{B}_{\text{line}}\Delta\boldsymbol{v}_{\text{blineDQ}} + \boldsymbol{B}_{\text{line+\_pcc}}\Delta\boldsymbol{v}_{\text{pccDQ}} + \boldsymbol{B}_{\text{lineDE}}\Delta\omega_{\text{ref}}$$
$$\Delta\boldsymbol{x}_{\text{line}} = [+\mathbf{I}_{6\times 6}]\Delta\boldsymbol{x}_{\text{line}} \tag{1}$$

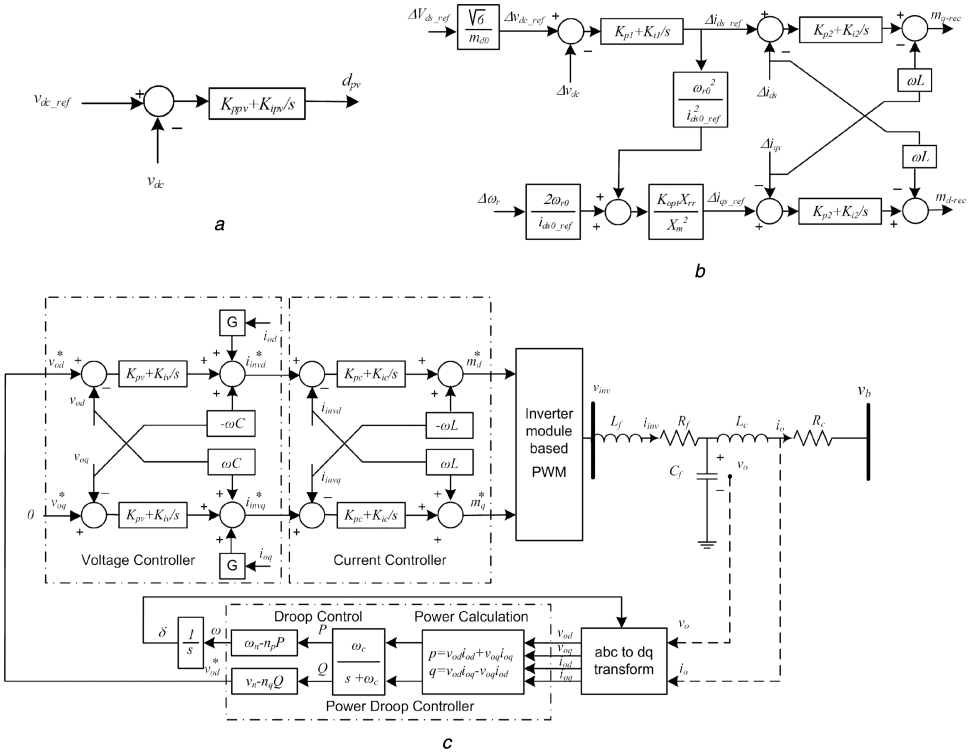

Fig. 2 *Generator side control*
(a) DC/DC converter control of PV system, ***(b)*** FOC of WECS, ***(c)*** Grid side DC/AC inverter control for PV and WECS

$$\begin{aligned}\Delta\dot{\boldsymbol{\rho}}_{\text{pv}} &= [0]\Delta\rho_{\text{pv}} + [1 \quad -1]\begin{bmatrix}\Delta v_{\text{dc\_ref}} \\ \Delta v_{\text{dc}}\end{bmatrix} \\ \Delta\boldsymbol{d}_{\text{pv}} &= [K_{\text{ipv}}]\Delta\rho_{\text{pv}} + [K_{\text{ppv}} \quad -K_{\text{ppv}}]\begin{bmatrix}\Delta v_{\text{dc\_ref}} \\ \Delta v_{\text{dc}}\end{bmatrix}\end{aligned} \tag{7}$$

where $\Delta\rho_{\text{pv}}$ represents auxiliary variable of DC/DC controller. While $\Delta v_{\text{dc\_ref}}$ and Δd_{pv} represent the DC link reference voltage and DC/DC converter duty cycles, respectively.

The controller of grid side DC/AC inverter as depicted in Fig. 2*c* is divided into three parts: power droop, voltage and current controller. Power droop controller is mainly responsible for realising voltage regulation and power sharing scheme. Voltage controller loop is in charge of improving dynamic response and providing reference values for the current controller loop. Finally, the current controller generates control signals for DC/AC inverter.

2.3.1 Power droop controller: Power droop controller involves power calculation, low-pass filter and droop control blocks. Power calculation block calculates instantaneous active and reactive power from measured output current and voltage. To provide accurate power gain setting, first-order low-pass filter is employed to attenuate high-frequency components from DG output power. Power droop controller emulates governor operation in a synchronous machine to adjust the amount of active and reactive power injection from the corresponded DG. System frequency ($\Delta\omega$) and active power sharing are set by real power droop gain (n_p) while d-axis voltage reference (Δv^*_d) and reactive power sharing are determined by reactive power droop gain (n_q) as given by

$$\begin{aligned}\omega &= \omega_n - n_p\Delta p \\ v^*_{od} &= V_n - n_q\Delta q\end{aligned} \tag{8}$$

where (ω_n) and (V_n) represent nominal values of angular frequency and voltage, respectively.

Phase angle (δ) is determined from integral operation of the angular frequency (ω). q-axis voltage reference is assumed to be zero. Hence, state-space equations of power droop controller are presented by (see (9))

2.3.2 Voltage controller: State equation of voltage controller is given by (see (10)) where $\Delta\phi_{dq}$ represents the auxiliary variables in voltage controller. Δv^*_{dq}refers to the reference value of output voltage. Output variables from the voltage controller ($\Delta i^*_{\text{inv}d}$, $\Delta i^*_{\text{inv}q}$) are then applied to the inner current controller as reference values.

2.3.3 Current controller: The output of the current controller is modulation indices (m^*_d, m^*_q) as a control signal for DC/AC inverter. Current controller state equations are given by

$$\begin{bmatrix}\Delta\dot{\delta} \\ \Delta\dot{p} \\ \Delta\dot{q}\end{bmatrix} = \begin{bmatrix}0 & 0 & 0 \\ 0 & -\omega_c & 0 \\ 0 & 0 & -\omega_c\end{bmatrix}\begin{bmatrix}\Delta\delta \\ \Delta p \\ \Delta q\end{bmatrix} + \begin{bmatrix}0 & 0 & 0 & 0 \\ \omega_c I_{od} & \omega_c I_{oq} & \omega_c V_{od} & \omega_c V_{oq} \\ \omega_c I_{oq} & -\omega_c I_{od} & -\omega_c V_{oq} & \omega_c V_{od}\end{bmatrix}\begin{bmatrix}\Delta v_{od} \\ \Delta v_{oq} \\ \Delta i_{od} \\ \Delta i_{oq}\end{bmatrix} \tag{9}$$

$$\begin{bmatrix}\Delta\omega \\ \Delta v^*_d\end{bmatrix} = \begin{bmatrix}0 & -n_{p\text{pv}} & 0 \\ 0 & 0 & -n_{q\text{pv}}\end{bmatrix}\begin{bmatrix}\Delta\delta \\ \Delta p \\ \Delta q\end{bmatrix}$$

$$\begin{bmatrix}\Delta\dot{\beta}_d\\ \Delta\dot{\beta}_q\end{bmatrix}=[0]\begin{bmatrix}\Delta\beta_d\\ \Delta\beta_q\end{bmatrix}+\begin{bmatrix}1&0&-1&0\\0&1&0&-1\end{bmatrix}\begin{bmatrix}\Delta i^*_{\mathrm{inv}d}\\ \Delta i^*_{\mathrm{inv}q}\\ \Delta i_{\mathrm{inv}d}\\ \Delta i_{\mathrm{inv}q}\end{bmatrix}$$

$$\begin{bmatrix}\Delta m^*_d\\ \Delta m^*_q\end{bmatrix}=\begin{bmatrix}K_{\mathrm{i}c}&0\\0&K_{\mathrm{i}c}\end{bmatrix}\begin{bmatrix}\Delta\beta_d\\ \Delta\beta_q\end{bmatrix}+\begin{bmatrix}K_{\mathrm{p}c}&0&-K_{\mathrm{p}c}&-\omega_nL_f\\0&K_{\mathrm{p}c}&\omega_nL_f&-K_{\mathrm{p}c}\end{bmatrix}\begin{bmatrix}\Delta i^*_{\mathrm{inv}d}\\ \Delta i^*_{\mathrm{inv}q}\\ \Delta i_{\mathrm{inv}d}\\ \Delta i_{\mathrm{inv}q}\end{bmatrix} \tag{11}$$

where $\Delta\beta_d$ and $\Delta\beta_q$ represent auxiliary variables of the current controller.

A complete model of PV system is determined by combining state equations of DC/DC and DC/AC in [14, 15] and state equations of controllers in (7), (9), (10) and (11). Linearised state-space model of two-stage PV is given by (see (12)) where $\boldsymbol{u}_{\mathrm{pv}}=\begin{bmatrix}\Delta v_g & \Delta v^*_{\mathrm{dc}}\end{bmatrix}^{\mathrm{T}}$, $\boldsymbol{\Delta v}_{b1dq}=\begin{bmatrix}\Delta v_{b1d} & \Delta v_{b1q}\end{bmatrix}^{\mathrm{T}}$, $\boldsymbol{B}_{v\mathrm{pv}}=\begin{bmatrix}1/L_{i2}&0\\0&1/L_{i2}\end{bmatrix}$, $\boldsymbol{C}_{\mathrm{pv}}=\begin{bmatrix}0_{2\times16} & \mathbf{I}_{2\times2}\end{bmatrix}$

Output currents of PV system have to be aligned with common reference frame as stated by

$$\boldsymbol{\Delta i}_{o\mathrm{pv}DQ}=\boldsymbol{C}_{\mathrm{pv}DQ}\boldsymbol{\Delta x}_{\mathrm{pv}} \tag{13}$$

where $\boldsymbol{C}_{\mathrm{pv}DQ}=\begin{bmatrix}0_{2\times5} & \mathbf{T}_{c\delta\mathrm{pv}} & 0_{2\times10} & \mathbf{T}_{c\mathrm{pv}}\end{bmatrix}$.

Input variables of the proposed PV model in (12) are represented by the input voltage of PV array, reference DC link voltage (Δv^*_{dc}), local bus voltages and $\Delta\omega_{\mathrm{ref}}$. Substitution of (3)and (13) into (12) provide complete PV state-space model. Hence, the state-space PV model in (12) can be further modified as

$$\begin{aligned}\boldsymbol{\Delta\dot{x}}_{\mathrm{pv}}&=\left(\boldsymbol{A}_{\mathrm{pv}}+R_N\boldsymbol{B}_{v\mathrm{pv}}\boldsymbol{C}_{\mathrm{pv}DQ}\right)\boldsymbol{\Delta x}_{\mathrm{pv}}+\boldsymbol{B}_{\mathrm{pv}}\boldsymbol{\Delta u}_{\mathrm{pv}}\\&+\boldsymbol{B}_{\mathrm{pvline}}\boldsymbol{\Delta x}_{\mathrm{line}}+\boldsymbol{B}_{\mathrm{pvDE}}\boldsymbol{\Delta x}_{\mathrm{DE}}\end{aligned} \tag{14}$$

where $\boldsymbol{B}_{\mathrm{pvline}}=R_N\begin{bmatrix}\boldsymbol{B}_{v\mathrm{pv}} & 0_{18\times4}\end{bmatrix}$, $\boldsymbol{B}_{\mathrm{pvde}}+=\boldsymbol{B}_{v\mathrm{pv}}\boldsymbol{C}_{\mathrm{de}2}$.

2.4 WECS model

State-space model of fully rated WECS mainly consists of a wind turbine, induction generator, back-to-back AC/DC/AC inverter and associated controllers. State-space model of AC/DC/AC is constructed by integrating AC/DC rectifier and DC/AC inverter model from [16, 17] and [15], respectively. Induction generator model is derived from [12, 13]. State variables of the induction machine are comprising of the stator (i_{sd}, i_{sq}) and rotor current (i_{rd}, i_{rq}). While input variables are stator (v_{sd}, v_{sq}) and rotor (v_{rd}, v_{rq}) voltage. The model is completed by mechanical equations and electromagnetic torque equation.

Flux oriented control (FOC) method as depicted in Fig. 2*b* was applied to the generator side AC/DC rectifier [18]. The control method supports variable speed operation capability of induction generator and maintains the stable condition of the terminal generator and DC link voltage. In this paper, DC link and generator terminal voltage are controlled by adjusting switching action of AC/DC rectifier. Reference of DC link voltage is determined from *d*-axis stator voltage reference and nominal modulation index of AC/DC rectifier which can be obtained from this following equation [19]:

$$V_{\mathrm{DC}\_ref}=\frac{\sqrt{6}V_{ds\_\mathrm{ref}}}{m_{d0\_\mathrm{rec}}} \tag{15}$$

The difference between the reference and measured DC link voltage is regulated through PI controller. The output of this controller yield reference of *d*-axis stator current (i^*_{ds}). State equation of FOC can be stated as

$$\begin{aligned}[\Delta\dot{\gamma}]&=[0]\Delta\gamma+[-1]\Delta v_{d\mathrm{cout}}+\left[\frac{\sqrt{6}}{m_{d0}}\right]\Delta v_{ds\_\mathrm{ref}}\\ \Delta i^*_{ds}&=[K_{i1}]\Delta\gamma+\left[-K_{p1}\right]\Delta v_{d\mathrm{cout}}+\left[\frac{K_{p1}\sqrt{6}}{m_{d0}}\right]\Delta v_{ds\_\mathrm{ref}}\end{aligned} \tag{16}$$

q-axis reference current (i^*_{qs}) is obtained based on a torque-speed characteristic curve. Electromagnetic torque equation can be simplified by assuming that rotor flux of induction generator is aligned with the direct axis ($\psi_{qr}=0$) and optimal operation of a wind turbine is attained [18]. The linearised *q-axis* reference current can be calculated as

$$\begin{aligned}\Delta i^*_{qs}=&\left(\frac{2\omega_{r0}K_{\mathrm{opt}}X_{rr}}{i^*_{d0s}X^2_m}\right)\Delta\omega_r+\left(\frac{K_{i1}K_{\mathrm{opt}}\omega^2_{r0}X_{rr}}{\left(i^*_{d0s}\right)^2X^2_m}\right)\Delta\gamma\\&-\left(\frac{K_{p1}K_{\mathrm{opt}}\omega^2_{r0}X_{rr}}{\left(i^*_{d0s}\right)^2X^2_m}\right)\Delta v_{d\mathrm{cout}}+\left(\frac{K_{p1}K_{\mathrm{opt}}\omega^2_{r0}X_{rr}\sqrt{6}}{\left(i^*_{d0s}\right)^2X^2_Mm_{d0}}\right)\Delta v_{ds\_\mathrm{ref}}\end{aligned} \tag{17}$$

where X_{rr} and X_m constitute rotor and mutual inductance of generator, respectively.

Obtained reference currents are compared with the measured *q*-axis stator current for generating a control signal of AC/DC

$$\begin{bmatrix}\Delta\dot{\varphi}_d\\ \Delta\dot{\varphi}_q\end{bmatrix}=[0]\begin{bmatrix}\Delta\varphi_d\\ \Delta\varphi_q\end{bmatrix}+\begin{bmatrix}1&0&-1&0\\0&1&0&1\end{bmatrix}\begin{bmatrix}\Delta v^*_{od}\\ \Delta v^*_{oq}\\ \Delta v_{od}\\ \Delta v_{oq}\end{bmatrix}$$

$$\begin{bmatrix}\Delta i^*_{\mathrm{inv}d}\\ \Delta i^*_{\mathrm{inv}q}\end{bmatrix}=\begin{bmatrix}K_{\mathrm{iv}}&0\\0&K_{\mathrm{iv}}\end{bmatrix}\begin{bmatrix}\Delta\varphi_d\\ \Delta\varphi_q\end{bmatrix}+\begin{bmatrix}K_{\mathrm{pv}}&0&-K_{\mathrm{pv}}&-\omega_nC_f&G&0\\0&K_{\mathrm{pv}}&\omega_nC_f&-K_{\mathrm{pv}}&0&G\end{bmatrix}\begin{bmatrix}\Delta v^*_{od}\\ \Delta v^*_{oq}\\ \Delta v_{od}\\ \Delta v_{oq}\\ \Delta i_{od}\\ \Delta i_{oq}\end{bmatrix} \tag{10}$$

$$\begin{aligned}\boldsymbol{\Delta\dot{x}}_{\mathrm{pv}}&=A_{\mathrm{pv}}\boldsymbol{\Delta x}_{\mathrm{pv}}+\boldsymbol{B}_{\mathrm{pv}}\boldsymbol{\Delta u}_{\mathrm{pv}}+\boldsymbol{B}_{v\mathrm{pv}}\boldsymbol{\Delta v}_{b2}+\boldsymbol{B}_{\omega\mathrm{pv}}\Delta\omega_{\mathrm{ref}}\\ \boldsymbol{\Delta x}_{\mathrm{pv}}&=[\Delta i_b\quad\Delta i_s\quad\Delta v_b\quad\Delta v_{\mathrm{dc}}\quad\Delta\rho_{\mathrm{pv}}\quad\Delta\delta_{\mathrm{pv}}\quad\Delta p_{\mathrm{pv}}\quad\Delta q_{\mathrm{pv}}\quad\Delta\varphi_{\mathrm{pv}d}\quad\Delta\varphi_{\mathrm{pv}q}\\&\quad\Delta\beta_{\mathrm{pv}d}\quad\Delta\beta_{\mathrm{pv}q}\quad\Delta i_{id}\quad\Delta i_{iq}\quad\Delta v_{od}\quad\Delta v_{oq}\quad\Delta i_{od}\quad\Delta i_{oq}]^{\mathrm{T}}\\ \boldsymbol{\Delta i}_{o\mathrm{pv}dq}&=\boldsymbol{C}_{\mathrm{pv}}\boldsymbol{\Delta x}_{\mathrm{pv}}\end{aligned} \tag{12}$$

converter (m_{d_rec}, m_{q_rec}). By integrating (16) and (17), state equations of FOC are given by (see (18)) where $\Delta\rho_{dq}$ represent auxiliary variable in FOC controller.

$$\boldsymbol{B}_{\mathrm{lFOC}} = \begin{bmatrix} -1 & 0 & K_{i1} & -K_{p1} & 0 \\ 0 & -1 & \dfrac{K_{i1}K_{\mathrm{opt}}\omega_{r0}^2 X_{rr}}{(i_{d0s}^*)^2 X_m^2} & -\dfrac{K_{p1}K_{\mathrm{opt}}\omega_{r0}^2 X_{rr}}{(i_{d0s}^*)^2 X_m^2} & \dfrac{2\omega_{r0}^2 K_{\mathrm{opt}} X_{rr}}{(i_{d0s}^*)^2 X_m^2} \end{bmatrix},$$

$$\boldsymbol{B}_{\mathrm{FOC2}} = \begin{bmatrix} \dfrac{K_{p1}\sqrt{6}}{m_{d0}} \\ \dfrac{K_{p1}K_{\mathrm{opt}}\omega_{r0}^2 X_{rr}\sqrt{6}}{(i_{d0s}^*)^2 X_m^2 m_{d0}} \end{bmatrix}$$

$$\boldsymbol{D}_{\mathrm{FOC1}} = \begin{bmatrix} -K_{p2} & -\omega L & K_{i1} & -K_{p1}K_{p2} \\ \omega L & -K_{p2} & \dfrac{K_{i1}K_{p2}K_{\mathrm{opt}}\omega_{r0}^2 X_{rr}}{(i_{d0s}^*)^2 X_m^2} & -\dfrac{K_{p1}K_{p2}K_{\mathrm{opt}}\omega_{r0}^2 X_{rr}}{(i_{d0s}^*)^2 X_m^2} \end{bmatrix},$$

$$\boldsymbol{D}_{\mathrm{FOC2}} = \begin{bmatrix} 0 \\ \dfrac{2\omega_{r0}K_{p2}K_{\mathrm{opt}}X_{rr}}{(i_{d0s}^*)^2 X_m^2} \end{bmatrix}, \boldsymbol{D}_{\mathrm{FOC3}} = \begin{bmatrix} \dfrac{K_{i1}K_{p2}\sqrt{6}}{m_{d0}} \\ \dfrac{K_{p1}K_{p2}K_{\mathrm{opt}}\omega_{r0}^2 X_{rr}\sqrt{6}}{(i_{d0s}^*)^2 X_m^2 m_{d0}} \end{bmatrix}$$

Similar control algorithm as grid side DC/AC inverter in two-stage PV as depicted in Fig. 2*c* was adopted to develop the grid side inverter control in WECS. Complete state-space model for fully rated converter WECS is then derived from the integration of induction generator model in [12, 13], back-to-back inverter model in [15–17], FOC in (18) and grid side inverter control in (9), (10) and (11). Linearised state-space equations of WECS presented as given by

$$\Delta\dot{\boldsymbol{x}}_w = A_w\Delta\boldsymbol{x}_w + \boldsymbol{B}_w\Delta\boldsymbol{u}_w + \boldsymbol{B}_{vw}\Delta\boldsymbol{v}_{b1} + \boldsymbol{B}_{w\mathrm{DE}}\Delta\omega_{\mathrm{ref}} \tag{19}$$

where (see equation below)

$$\Delta\boldsymbol{v}_{b1} = \begin{bmatrix}\Delta v_{b1d} & \Delta v_{b1q}\end{bmatrix}^{\mathrm{T}}, \boldsymbol{B}_{vw} = \begin{bmatrix} 1/L_{i1} & 0 \\ 0 & 1/L_{i1} \end{bmatrix}, \ \boldsymbol{C}_w = \begin{bmatrix} 0_{2\times 26} & \boldsymbol{I}_{2\times 2} \end{bmatrix}$$

Input state variables of WECS are stator ($\Delta v_{\mathrm{s}dq}$) and rotor ($\Delta v_{\mathrm{r}dq}$) voltage, mechanical input torque (ΔT_w) and FOC reference stator voltage ($\Delta v^*_{\mathrm{s}d}$). Output current of this DG in common reference frame is given by

$$\Delta\boldsymbol{i}_{owDQ} = \boldsymbol{C}_{wDQ}\Delta\boldsymbol{x}_w \tag{20}$$

where $\boldsymbol{C}_{wDQ} = \begin{bmatrix} 0_{2\times 13} & \mathbf{T}_{c\delta w} & 0_{2\times 12} & \mathbf{T}_{cw} \end{bmatrix}$.

Similar procedure as in PV system is conducted to determine the connection between WECS, DE and line impedance. The complete state-space model of WECS can be stated by

$$\Delta\dot{\boldsymbol{x}}_w = (\boldsymbol{A}_w + R_N\boldsymbol{B}_{vw}\boldsymbol{C}_{wDQ})\Delta\boldsymbol{x}_w + \boldsymbol{B}_w\Delta\boldsymbol{u}_w + \boldsymbol{B}_{w\mathrm{line}}\Delta\boldsymbol{x}_{\mathrm{line}} + \boldsymbol{B}_{w\mathrm{DE}}\Delta\boldsymbol{x}_{\mathrm{de}} \tag{21}$$

where $\boldsymbol{B}_{w\mathrm{line}} = R_N\begin{bmatrix} 0_{25\times 2} & \boldsymbol{B}_{vw} & 0_{25\times 2} \end{bmatrix}, \boldsymbol{B}_{wde} = \boldsymbol{B}_{vw}\boldsymbol{C}_{de2}$.

2.5 Connection of lines impedance to DG units and central load

Input variables of state-space model in (1) indicate the connection of the lines to the output of DG units and central load. By substituting (3) and (4) to (1), complete state-space model of line impedance is given by

$$\Delta\dot{\boldsymbol{x}}_{\mathrm{line}} = \left\{\boldsymbol{A}_{\mathrm{line}} + R_N\left(\boldsymbol{B}_{\mathrm{line\_pcc}}\boldsymbol{C}_{\mathrm{lilo}} - \boldsymbol{B}_{\mathrm{line}}\right)\right\}\Delta\boldsymbol{x}_{\mathrm{line}} + \boldsymbol{B}_{\mathrm{lipv}}\Delta\boldsymbol{x}_{\mathrm{pv}} + \boldsymbol{B}_{\mathrm{liw}}\boldsymbol{x}_w + \boldsymbol{B}_{\mathrm{lineDE}}\Delta\boldsymbol{x}_{de} + \boldsymbol{B}_{\mathrm{linelo}}\Delta\boldsymbol{x}_{\mathrm{load}} \tag{22}$$

where (see equation below)

2.6 Connection of load to DG units and line impedances

Complete equation of central load is determined by substituting (4) to (2) as stated by

$$\Delta\dot{\boldsymbol{x}}_{\mathrm{lo}} + = \boldsymbol{A}_{\mathrm{lo}}\Delta\boldsymbol{x}_{\mathrm{lo}} + \boldsymbol{B}_{\mathrm{loli}}\Delta\boldsymbol{x}_{\mathrm{line}} + \boldsymbol{B}_{\mathrm{loDE}}\boldsymbol{C}_{\mathrm{lDE2}}\Delta\boldsymbol{x}_{\mathrm{DE}} \tag{23}$$

where $\boldsymbol{B}_{\mathrm{loli}} = R_N\boldsymbol{B}_{\mathrm{lo}}\boldsymbol{C}_{\mathrm{lilo}}$, $\boldsymbol{B}_{\mathrm{loDE}} = \boldsymbol{C}_{\mathrm{lDE2}}\Delta\boldsymbol{x}_{\mathrm{DE}}$.

2.7 Comprehensive state-space model of MG

Three MG structures that consist of two RES-based DGs and one DE are considered. Full state-space model of the studied MG is derived by combining state equations of DGs, lines and load. In general, linearised state-space model of MG is given by

$$\Delta\dot{\boldsymbol{x}}_{\mathrm{MG}} = \boldsymbol{A}_{\mathrm{MG}}\Delta\boldsymbol{x}_{\mathrm{MG}} + \boldsymbol{B}_{\mathrm{MG}}\Delta\boldsymbol{u}_{\mathrm{MG}} \tag{24}$$

where $\Delta\boldsymbol{x}_{\mathrm{MG}} = \begin{bmatrix}\Delta\boldsymbol{x}_{\mathrm{DG1}} & \Delta\boldsymbol{x}_{\mathrm{DG2}} & \Delta\boldsymbol{x}_{\mathrm{DE}} & \Delta\boldsymbol{x}_{\mathrm{line}} & \Delta\boldsymbol{x}_{\mathrm{load}}\end{bmatrix}^{\mathrm{T}}$, $\Delta\boldsymbol{u}_{\mathrm{MG}} = \begin{bmatrix}\Delta\boldsymbol{u}_{\mathrm{DG1}} & \Delta\boldsymbol{u}_{\mathrm{DG2}} & \Delta\boldsymbol{u}_{\mathrm{DE}}\end{bmatrix}^{\mathrm{T}}$

$$\boldsymbol{B}_{\mathrm{MG}} = \begin{bmatrix} \boldsymbol{B}_{\mathrm{DG1}} & 0 & 0 \\ 0 & \boldsymbol{B}_{\mathrm{DG2}} & 0 \\ 0 & 0 & \boldsymbol{B}_{\mathrm{DE}} \end{bmatrix},$$

$$\boldsymbol{A}_{\mathrm{MG}} = \begin{bmatrix} \boldsymbol{A}_{11} & 0 & \boldsymbol{B}_{\mathrm{DG1DE}} & \boldsymbol{B}_{\mathrm{DG1line}} & 0 \\ 0 & \boldsymbol{A}_{22} & \boldsymbol{B}_{\mathrm{DG2DE}} & \boldsymbol{B}_{\mathrm{DG2line}} & 0 \\ 0 & 0 & \boldsymbol{A}_{33} & \boldsymbol{B}_{\mathrm{DEline}} & 0 \\ \boldsymbol{B}_{\mathrm{liDG1}} & \boldsymbol{B}_{\mathrm{liDG2}} & \boldsymbol{B}_{\mathrm{lineDE}} & \boldsymbol{A}_{44} & \boldsymbol{B}_{\mathrm{lilo}} \\ 0 & 0 & \boldsymbol{B}_{\mathrm{loDE}} & \boldsymbol{B}_{\mathrm{lilo}} & \boldsymbol{A}_{55} \end{bmatrix}$$

$$\begin{aligned} \boldsymbol{A}_{11} &= \boldsymbol{A}_{\mathrm{DG1}} + R_N\boldsymbol{B}_{v\mathrm{DG1}}\boldsymbol{C}_{\mathrm{DG1DQ}} \\ \boldsymbol{A}_{22} &= \boldsymbol{A}_{\mathrm{DG2}} + R_N\boldsymbol{B}_{v\mathrm{DG2}}\boldsymbol{C}_{\mathrm{DG2DQ}} \\ \boldsymbol{A}_{33} &= \boldsymbol{A}_{\mathrm{DE}} + R_N\boldsymbol{B}_{v\mathrm{DE}}\boldsymbol{C}_{\mathrm{DE1}} \\ \boldsymbol{A}_{44} &= \boldsymbol{A}_{\mathrm{line}} + R_N\left(\boldsymbol{B}_{\mathrm{line\_pcc}}\boldsymbol{C}_{\mathrm{lilo}} - \boldsymbol{B}_{\mathrm{line}}\right) \\ \boldsymbol{A}_{55} &= \boldsymbol{A}_{\mathrm{lo}} \end{aligned}$$

where DG1 and DG2 notations represent RES-based DGs as depicted in Fig. 1.

3 Small signal stability analysis and identification of modal interaction

3.1 Small signal stability

Eigen-properties of state matrix reveal valuable information regarding system stability after being subjected to a small perturbation. The eigenvalues of state matrix provide an accurate estimation of system stability performance. Complex eigenvalues (λ) indicate oscillatory frequency (f) and damping ratio (ζ) of critical modes as follows:

$$\begin{aligned} \lambda_i &= \sigma_i \pm \mathrm{j}\omega_i \\ f &= \omega_i/2\pi \\ \zeta &= -\sigma_i/\sqrt{\sigma_i^2 + \omega_i^2} \end{aligned} \tag{25}$$

3.2 Identification of modal interaction

Interaction among eigenvalues might emerge in a stressed power system under heavy loading or small system damping conditions [20]. In those circumstances, some sensitive modes might be situated firmly and potentially interact. As a result, deterioration of system damping indicated by more oscillatory condition possibly happen. In this paper, three analytical methods are used to identify and confirm the occurrence of modal interaction which could be one of the mechanisms to instability.

3.2.1 Observation of eigen-trajectories: Modal interaction is characterised by a particular eigen-trajectories of the engaged modes. The simplest procedure to identify the occurrence of interaction is by monitoring the eigenvalues movement. Primarily, two or more interacting modes were approaching close together. When the interacting modes situated around an interaction point, the corresponded modes are extremely sensitive to parameter variations or disturbance. After approaching interaction point, the involved modes departed quickly and deviate significantly [4, 9, 11, 21], and result in deterioration of system stability.

3.2.2 Cross-participation factor: Participation factor corresponded to the relative contribution of the kth state variables in a particular ith eigenvalues. Let participation factor of kth state variables in ith modes is denoted by p_{ki} and defined as

$$p_{ki} = \phi_{ki}\psi_{ki} \tag{26}$$

where ϕ_{ki} and ψ_{ki}, respectively, represent the kth element on the right eigenvector and left eigenvector in ith modes.

The interaction among neighbouring eigenvalues can be recognised by observing contribution of state variables in the engaged modes [10]. The interaction between two modes is expected when CPF is identified. CPF is defined as the involvement of states variables in both of the interacting eigenvalues [8]. The occurrence of interaction is confirmed when at least one state variable participates in each of the interacting modes. Far from the interaction point, the cross-participation values are relatively small. When the engaged modes moved closer and approached the interaction point, the CPT increased gradually and reached the highest values at the nearest distance around the interaction point. The CPT would decrease significantly as the interacting modes were leaving the resonance point.

3.2.3 Modal interaction index (MII): Activity and contribution of state variables x_k in the dynamic response of ith mode can be represented by the kth element of right ($\boldsymbol{\phi}_i$) and left ($\boldsymbol{\psi}_i$) eigenvectors, respectively [22]. Therefore, dynamic response of state variables is stated in this following equation [22]:

$$x(t) = \sum_{i=1}^{n} \boldsymbol{\phi}_i\boldsymbol{\psi}_i\Delta x_i(0)e^{\lambda_i t} \tag{27}$$

For a particular state variable of x_k, the dynamic response of the corresponded modes is given by

$$x_k(t) = \sum_{i=1}^{n} \boldsymbol{\phi}_i\boldsymbol{\psi}_i\Delta x_{ki}(0)e^{\lambda_i t} \tag{28}$$

According to (28), more oscillatory condition as a consequence of modal interaction is reflected by increasing values of right and left eigenvector product. A novel index namely MII is considered to provide more accurate identification method for modal interaction. The proposed index identifies occurrence and quantifies the extent of interaction. MII between two engaged modes of λ_i and λ_j is characterised by eigenvector product as

$$\text{MII} = \boldsymbol{\psi}_i\phi_j + \psi_j\boldsymbol{\phi}_i \tag{29}$$

Higher values of MII indicated the occurrence of stronger modal interaction. MII can vary between 0 and $\text{MII}_{\max}$ denoting the condition of modal interaction. In the normalised form, the maximum value of left and right eigenvector product is one. Since the proposed index comprising of two parts product of left and right eigenvector, $\text{MII}_{\max}$ is decided equal to 1. This situation occurred when two eigenvalues exactly coincided in one interaction point. The normalised form of MII can be stated in the following equation:

$$\begin{bmatrix}\Delta\dot{\rho}_d\\ \Delta\dot{\rho}_q\end{bmatrix} = \begin{bmatrix}0 & 0\\ 0 & 0\end{bmatrix}\begin{bmatrix}\Delta\rho_d\\ \Delta\rho_q\end{bmatrix} + \boldsymbol{B}_{1\text{FOC}}\begin{bmatrix}i_{ds}\\ i_{qs}\\ \Delta\gamma\\ \Delta v_{\text{dc}}\\ \Delta\omega\end{bmatrix} + \boldsymbol{B}_{2\text{FOC}}[\Delta v_{ds}^*]$$
$$\begin{bmatrix}\Delta m_{d\_\text{rec}}\\ \Delta m_{q\_\text{rec}}\end{bmatrix} = \begin{bmatrix}K_{i2} & 0\\ 0 & K_{i2}\end{bmatrix}\begin{bmatrix}\Delta\rho_d\\ \Delta\rho_q\end{bmatrix} + \boldsymbol{D}_{\text{FOC}1}\begin{bmatrix}\Delta i_{ds}^*\\ \Delta i_{qs}^*\\ \Delta i_{ds}\\ \Delta i_{qs}\end{bmatrix} + \boldsymbol{D}_{\text{FOC}2}[\Delta\omega_r] + \boldsymbol{D}_{\text{FOC}3}[\Delta v_{ds}^*] \tag{18}$$

$$\begin{aligned}\Delta\boldsymbol{x}_w = [&\Delta i_{sd}\ \ \Delta i_{sq}\ \ \Delta i_{rd}\ \ \Delta i_{rq}\ \ \Delta\omega_r\ \ \Delta\gamma\ \ \Delta\rho_d\ \ \Delta\rho_q\\ &\Delta i_{id}\ \ \Delta i_{iq}\ \ \Delta v_{d\text{in}}\ \ \Delta v_{q\text{in}}\ \ \Delta v_{\text{dcout}}\ \ \Delta\delta\ \ \Delta p\ \ \Delta q\ \ \Delta\varphi_d\ \ \Delta\varphi_q\\ &\Delta\beta_d\ \ \Delta\beta_q\ \ \Delta i_s\ \ \Delta v_{\text{dc}}\ \ \Delta i_{\text{inv}d}\ \ \Delta i_{\text{inv}q}\ \ \Delta v_{od}\ \ \Delta v_{oq}\ \ \Delta i_{od}\ \ \Delta i_{oq}]^{\text{T}}\\ \Delta\boldsymbol{i}_{odq} = \boldsymbol{C}_w\Delta\boldsymbol{x}_w,\ &\Delta\boldsymbol{u}_w = [\Delta v_{sd}\ \ \Delta v_{sq}\ \ \Delta v_{rd}\ \ \Delta v_{rq}\ \ \Delta T_w\ \ \Delta v_{sd}^*]^{\text{T}}\end{aligned}$$

$$\boldsymbol{C}_{\text{lilo}} = \begin{bmatrix}1 & 0 & 1 & 0 & 1 & 0\\ 0 & 1 & 0 & 1 & 0 & 1\end{bmatrix},\ \boldsymbol{B}_{\text{lipv}} = R_N\begin{bmatrix}\boldsymbol{B}_{\text{li}1}\\ 0_{4\times 2}\end{bmatrix}\boldsymbol{C}_{\text{pv}},$$
$$\boldsymbol{B}_{\text{liw}} = R_N\begin{bmatrix}0_{2\times 2}\\ \boldsymbol{B}_{\text{li}2}\\ 0_{2\times 2}\end{bmatrix}\boldsymbol{C}_w,\ \boldsymbol{B}_{\text{lineDE}} = \begin{bmatrix}0_{4\times 2}\\ \boldsymbol{B}_{\text{li}3}\end{bmatrix}\boldsymbol{C}_{\text{de}1} + \boldsymbol{B}_{\text{lineDE}}\boldsymbol{C}_{\text{de}2}+,\ \boldsymbol{B}_{\text{lilo}} = R_N\boldsymbol{B}_{\text{line\_pcc}}$$

Table 1 Sensitive eigenvalues in MG architectures

MG architectures	Sensitive modes, λ	Frequency, Hz	Damping, ζ	Participation factor
MG1: 2-WECS 1-DE MG				
WECS-1 ($\lambda_{50,51}$)	−2.88 ± i11.35	1.81	24.59%	P_{WECS1}, δ_{WECS1}, Q_{WECS1}
WECS-2 ($\lambda_{52,53}$)	−0.43 ± i9.08	1.44	4.73%	P_{WECS2}, δ_{WECS2}, Q_{WECS2}
MG2: 2-PV 1-DE MG				
PV-1 ($\lambda_{36,37}$)	−3.98 ± i4.61	0.73	65.34%	P_{PV1}, δ_{PV1}, Q_{PV1}, P_{PV2}, δ_{PV2}, Q_{PV2}
PV-2 ($\lambda_{38,39}$)	−1.41 ± i4.41	0.70	30.45%	P_{PV2}, δ_{PV2}, Q_{PV2}, P_{PV1}, δ_{PV1}, Q_{PV1}
MG3: WECS, PV, DE MG				
WECS ($\lambda_{42,43}$)	−1.67 ± i8,51	1.36	19.25%	P_{WECS}, δ_{WECS}, Q_{WECS}, P_{PV}, δ_{PV}, Q_{PV}
PV ($\lambda_{45,46}$)	−0.49 ± 10.44	1.66	4.71%	P_{PV}, δ_{PV}, Q_{PV}, P_{WECS}, δ_{WECS}, Q_{WECS}

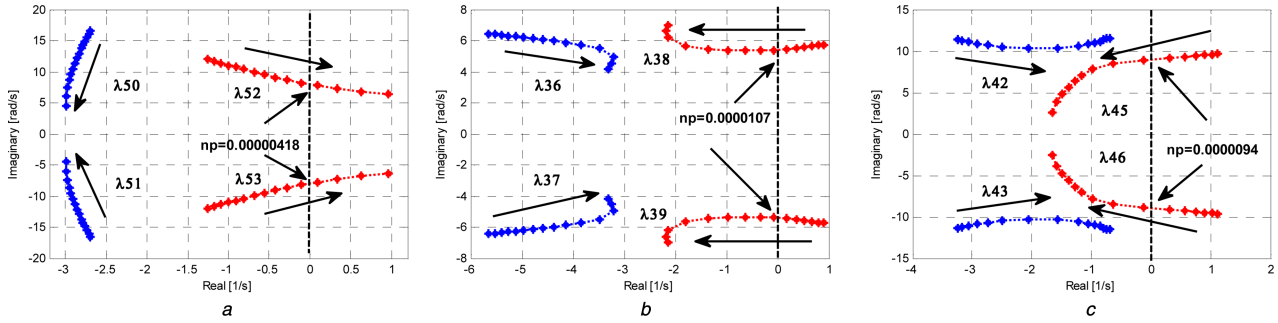

Fig. 3 *Trajectories of sensitive modes when n_p varied from 1.57×10^{-5} to 1.05×10^{-6} in*
(a) MG1: 2-WECS 1-DE MG, ***(b)*** MG2: 2-PV 1-DE MG, ***(c)*** MG3: hybrid WECS PV DE MG

$$\text{Norm\_MII} = \frac{\psi_i\phi_j + + \psi_j\phi_i}{\sqrt{\sum_{k=1}^{n}(\psi_k^2)}\sqrt{\sum_{k=1}^{n}(\phi_k^2)}} \tag{30}$$

where Norm_MII and n are the normalised MII and the number of state variables, respectively.

4 Results and discussions

4.1 Small signal stability

4.1.1 Eigenvalues analysis: A complete state-space model of three MG architectures as depicted in Fig. 1 is considered. In each MG structure, 5 MW load is supplied by two RES-based DG unit and DE. The MG1 architecture was represented by a 72-order model. While, MG2 and MG2 structures were represented by 52- and 62-order models, respectively. Parameters of WECS and DE were derived from [19, 12], respectively. Furthermore, power electronic devices, line impedances and load parameters are presented in Appendix.

This research is focused on sensitive modes which significantly influenced MG stability. The critical eigenvalues in the frequency range of 1–3 Hz are mainly originated from power sharing controller. It was assumed that modes associated with DE are asymptotically stable and did not contribute to the stability, hence only critical modes from WECS- and PV-based DGs were considered. Table 1 represents characteristics of the investigated modes of each MG structure. According to participation factor analysis, active power, phase angle and reactive power state variables from WECS and PV participated in those sensitive modes. $\lambda_{50,51}$ and $\lambda_{52,53}$ corresponded to sensitive modes from MG1. While the dynamic performance of MG2 and MG3 is represented by $\lambda_{36,37}$, $\lambda_{38,39}$ and $\lambda_{42,43}$, $\lambda_{45,46}$, respectively. It was observed that based on the eigenvalues analysis, overall critical modes from MG2 had much better damping ratio than other two MGs

Fig. 3 represents trajectories of the sensitive eigenvalues under variation of active power droop gain (n_p) and reactive power droop gain (n_q). As n_p decreased from 1.57×10^{-5} to 1.05×10^{-6}, the modes with higher damping ratio from MG2(a2) and MG3(a3) moved to the right, implies a deterioration of dynamic response. Moreover, only slight stability improvement was monitored in more damped modes from MG1(a1). Enhancement of stability was observed in MG2 and MG3 indicated by the left movement of eigenvalues of $\lambda_{38,39}$ and $\lambda_{45,46}$, respectively. However, a significant decrease of damping was observed in modes $\lambda_{52,53}$. Furthermore, oscillatory frequency of $\lambda_{45,46}$ drastically reduced from 7.408 rad/s or 1.17 Hz to 4.01 rad/s or 0.63 Hz. A similar trend was observed in the frequency of modes $\lambda_{50,51}$ which decreased significantly from 16.035 rad/s or 2.55 Hz to 4.36 rad/s or 0.69 Hz. On the other hand, the frequency of both sensitive modes in MG2 did not change significantly around 6.303 rad/s or 1.01 Hz as a result of gain variation.

As reactive power droop gain (n_q) was varied in the range of 0.0005–0.00001, enhancement of dynamic response was monitored, designated by left movement of $\lambda_{38,39}$ and $\lambda_{45,46}$ as depicted in Fig. 4*b*. While, the slight left motion of $\lambda_{42,43}$ as presented in Fig. 4*c* was observed during this variation. It was also monitored that deterioration of dynamic response occurred in MG2, indicated by the right movement of $\lambda_{36,37}$ in Fig. 4*b*. Moreover, Fig. 4*a* indicated that both of sensitive modes from MG1 were relatively fixed in their positions. Only small left movement of modes of $\lambda_{50,51}$ was monitored under n_q variation.

4.1.2 Time-domain simulation: The eigenvalue analyses were validated through time-domain simulations in MATLAB Simulink environment. To excite and investigate dynamic response of the observed modes, a small perturbation of input variables associated with a voltage reference of WECS (v^*_{ds}) and PV (v^*_{dc}) controllers were applied.

Fig. 5 represents dynamic response of RES-based DGs active power in three MG architectures at various n_p setting. In MG1, as depicted in Fig. 5*a*, the output power of WECS 1 and WECS 2 has a similar dynamic response. Primarily, the output power from WECS 1 and WECS oscillated in 1.67 and 1.43 Hz, respectively. According to previous modal analysis, the eigenvalues from WECS 1 had higher damping ratio than eigenvalues from WECS 2. Hence, the oscillatory condition of WECS 1 subsided immediately, and the corresponded modes started to oscillate in the range frequency of 1.43 Hz. A lower oscillatory state in MG2 was visualised in Fig. 5*b*. The corresponded active power from PV1 and PV2 DG

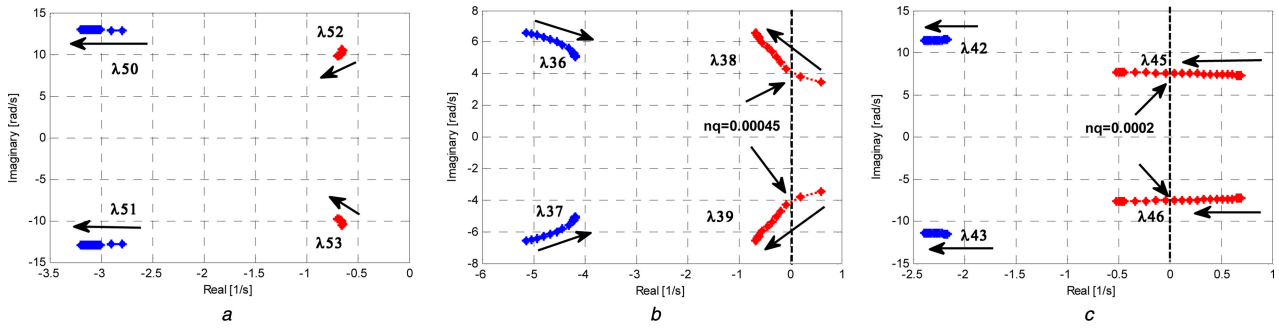

Fig. 4 *Trajectories of sensitive modes when n_q varied from 0.0005 to 0.00001 in*
(a) MG1: 2-WECS 1-DE MG, ***(b)*** MG2: 2-PV 1-DE MG, ***(c)*** MG3: hybrid WECS PV DE MG

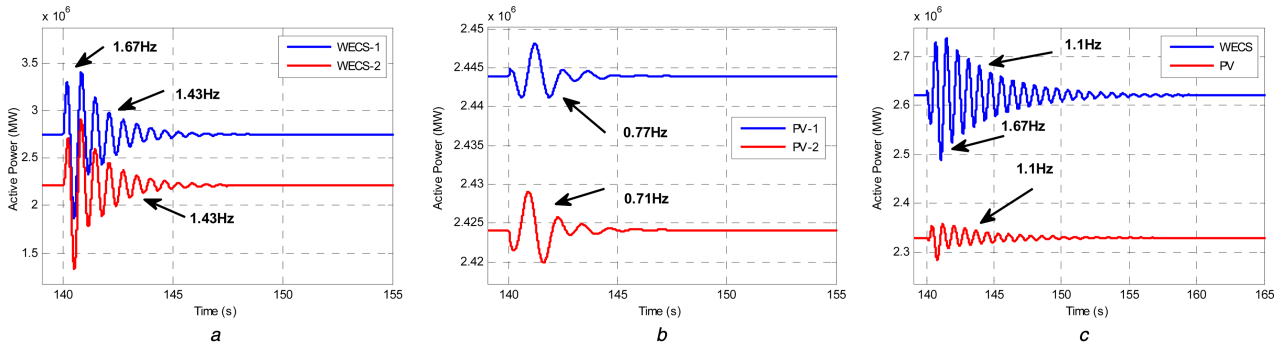

Fig. 5 *Active power of RES-based DGs at various setting of active droop gain (n_{pw}) in*
(a) MG1: 2-WECS 1-DE MG, ***(b)*** MG2: 2-PV 1-DE MG, ***(c)*** MG3: hybrid WECS PV DE MG

unit were oscillating at the frequency of 0.76 and 0.71 Hz, respectively.

Fig. 5*c* represents dynamic response of MG3. The output power of WECS and PV had an oscillatory frequency of 1.701 and 1.17 Hz, respectively. Primarily, WECS active power oscillated at the frequency of 1.67 Hz and PV power output oscillated at 1.1 Hz. Since the dynamic response of WECS damped instantaneously, both of the observed modes started to oscillate in the frequency around 1.1 Hz. This condition persisted until a stable operating point was achieved. Furthermore, it was noticeable that in hybrid system of MG3, WECS was characterised by less damped dynamic response than PV-based DG unit.

4.2 Identification of modal interaction

The following session provides identification procedures of modal interaction which potentially emerges due to non-linear behaviour of sensitive eigenvalues under a stressed condition, small disturbance and parameter variations. It could be a significant concern since it may cause a deterioration of system stability. In his paper, three analytical methods: observation of eigen-trajectories, CPT and MII are proposed to identify and confirm the event of eigen-interaction.

4.2.1 Observation of eigen-trajectories: Modal interaction is characterised by a typical eigenvalues movements. Hence, recognition of the interaction event can be approached through observation of eigenvalues trajectories. The engaged modes are approaching each other and coinciding in a particular point when an interaction took place. Around an interaction point, the interacting modes were very sensitive to parameter variations. After being aligned, the involved modes departed oppositely and may diverge in damping. Indeed, one of the eigenvalues potentially become unstable as a consequence of passing near an intense interaction [9].

One of the features in MG is a complex control system of each DGs. Tuning procedures of the gain controller of DG unit significantly influenced the behaviour of the sensitive eigenvalues. As a result, modal interaction possibly happened due to the variations. In this paper, proportional gain control of voltage (K_{pv}) and current controllers (K_{pc}) of RES-based DGs in each MG structure were varied to investigate possible occurrence of modal interaction. Fig. 6 depicts trajectories of the investigated modes under variation of n_p in a different setting of K_{pv} and K_{pc}. In Fig. 6*a*, it was monitored that at various gain setting, the eigen-trajectories did not deviate significantly. Hence, it can be considered only weak or negligible modal interaction event occurred in MG1. The occurrence of modal interactions in MG2 and MG3 were confirmed as depicted in Figs. 6*b* and *c*, respectively. It was shown that under a similar range of n_p variation, different setting of K_{pv} and K_{pc} introduced a significant impact on the eigen-trajectories. In both MGs, primarily, two interacting eigenvalues came closer together and interacted when K_{pv} and K_{pc} in MG2 and MG3 were tuned at 0.355 and 1.04, respectively. Around an interaction point, as marked by a circle, those two modes diverged significantly. One of the engaged modes departed to the left while the other one moved toward the right side, indicated enhancement and deterioration of system stability in those respective modes.

4.2.2 Cross-participation factor (CPF): Participation factor indicates activity and contribution of state variables in distinct eigenvalues. Hence, the modal interaction can be further confirmed through analysis of state variables contributions in the engaged modes. The interaction between two eigenvalues was expected when one or more state variables participated in both of engaged modes which can be defined as CPF.

Fig. 7 represents participation factor of the investigated modes in three MG structures. As depicted in Fig. 7*a*, CPF was not monitored in both modes. State variables from DG-1 only contributed in the modes-1 while state variables from DG-2 participated in the modes-2. Hence, it can be considered that modal interaction did not happen in MG1. This observation was confirmed by eigen-trajectories in Fig. 6*a*. CPF were identified in MG2 and MG3structures as shown in Figs. 7*b* and *c*, respectively. Away from the interaction point, CPF were relatively small. This situation confirmed an occurrence of weak interaction. When the engaged modes moved closer and approached an interaction point, CPF increased gradually and reached the highest values at the nearest distance around an interaction point. From the observed CPF values, moreover, it was monitored that the interaction event

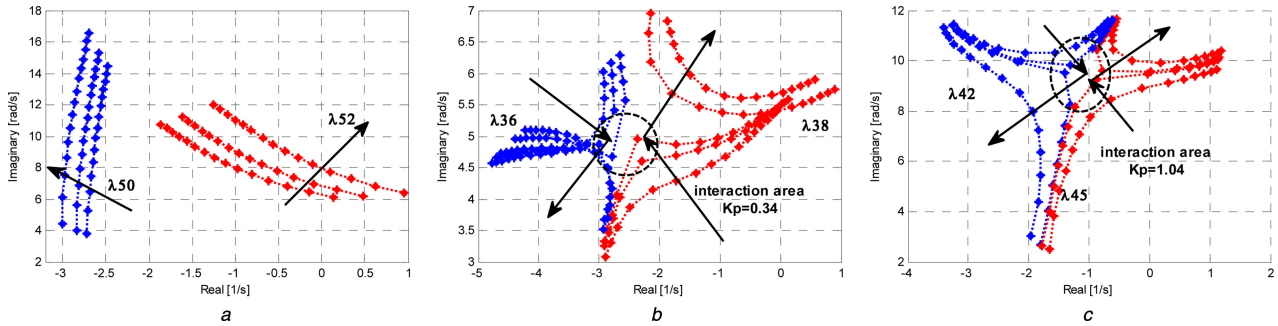

Fig. 6 *Trajectories of modes under variation of active power droop gain in various setting of voltage and current controller loops proportional gain in* ***(a)*** 2-WECS 1-DE MG, ***(b)*** 2-PV 1-DE MG, ***(c)*** Hybrid WECS PV DE MG

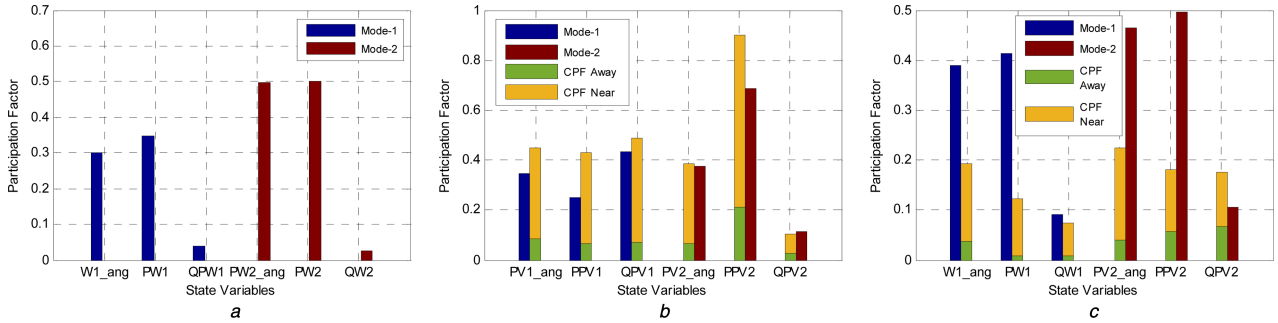

Fig. 7 *Participation factor of investigated modes in* ***(a)*** 2-WECS 1-DE MG, ***(b)*** 2-PV 1-DE MG, ***(c)*** Hybrid WECS PV DE MG

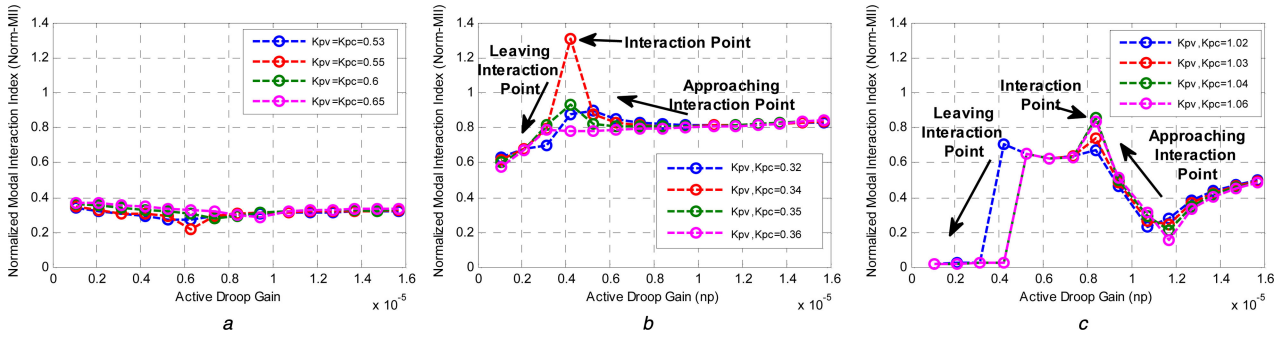

Fig. 8 *Normalised MII (Norm_MII) under variation of active power droop gain in different setting of voltage and current controller loops proportional gain in*
(a) 2-WECS 1-DE MG, ***(b)*** 2-PV 1-DE MG, ***(c)*** Hybrid WECS PV DE MG

in MG2 was more intense than in MG3 since, at the interaction point in MG2, all of the state variables relatively had similar participation factor in both of engaged modes. After interaction point, the involved eigenvalues deviated significantly hence the distance between two modes gradually increased which was reflected by the decrease of CPT in those corresponded modes.

4.2.3 Modal interaction index: Weak or neglected modal interaction is expected when the trajectories of the engaged modes did not deviate significantly. As a consequence, it was difficult to identify the occurrence of modal interaction through eigen-trajectories method. To overcome this limitation, identification method based on eigen-properties is needed to provide more accurate and sensitive detection of modal interaction. Hence, a normalised MII (Norm_MII) based on right and left eigenvector product as in (30) is proposed.

Fig. 8 represents Norm_MII of the interacting modes at different gain setting under a certain range of n_p variation. As shown in Fig. 8*a*, it was monitored that under K_{pv} and K_{pc} variation in MG1, small MII value was obtained and it did not change significantly during the changes. Hence, it can be considered that only weak or negligible modal interaction took place in the MG1. Conversely, strong modal interactions were identified in MG2 and MG3 as presented in Figs. 8*b* and *c*, respectively. The engaged modes in MG2 and MG3 primarily come closer together, indicated by a gradual increase of MII. Modes alignment was marked by a remarkable increase of MII. At the alignment point, the interacting modes nearly coincide in both of damping and frequency and were very sensitive to small variations. After coinciding, the engaged modes diverged oppositely, and the MII decreased significantly corresponded to weaker modal interaction. As indicated by the highest value of MII, the resonance point in MG2 occurred in the setting of droop gain control of 4.18×10^{-6} with K_{pv} and K_{pc} tuning of 0.34. While the interaction point in MG3 happened when the droop gain was tuned in 8.37×10^{-6} while K_{pv} and K_{pc} were set at 1.04.

According to Fig. 8, the MII in MG1 was smaller than MG2 and MG3. Hence, it was suggested that interaction in MG1 was much weaker than in MG2 and M3. That weak interaction was not identified by eigen-trajectories and cross-participation methods. However, the occurrence of weak interaction still could be detected by MII method. From the obtained result, it was notable that the MII method was more sensitive to identify the modal interaction event compared with eigen-trajectories and cross-participation methods.

5 Conclusions

A comprehensive model of WECS, PV and DE based DGs were presented to develop MG system. Since the different architecture of

DGs provided a distinct dynamic response, evaluation of MG stability in three distinct structures (2-WECS 1-DE, 2-PV 1-DE and WECS, PV, DE) were investigated. From MGs small signal stability performance, it was reported that low-frequency critical modes corresponded to DGs output power were very sensitive to gain controller variation. To ensure MGs stability during the autonomous mode of operation, stability boundaries of the MGs were determined under change of active and reactive power droop gains of power sharing strategies in MG. It was noticeable that different droop gain control settings may result in either enhancement or deterioration of system damping and dynamic responses.

Moreover, non-linear behaviour of sensitive modes in MGs potentially leads to the occurrence of modal interaction. In the investigated system, the interaction between two critical modes possibly happens due to the variation of gain parameters of inverter controllers. Interactions among sensitive modes were then monitored through three analytical methods. Significant deviation of eigen-trajectories, higher values of CPF and MII indicated occurrence of modal interaction event in the MGs. From three case studies in different MG architectures, it was emphasised that the proposed methodologies could be implemented as a framework for analysing, identifying and quantifying such potential modal interactions. Obtained result regarding the comprehensive analysis of small signal stability in autonomous operation and modal interaction identification methods contribute to the design consideration and stability margin prediction of hybrid MG system.

6 References

[1] Hatziargyriou, N., Hiroshi Asano, R.I., Marnay, A.C.: 'Microgrids: an overview of ongoing research, development, and demonstration projects'. IEEE Power and Energy Magazine, 2007, pp. 1540–7977

[2] Majumder, R.: 'Some aspects of stability in microgrids', *IEEE Trans. Power Syst.*, 2013, **28**, (3), pp. 3243–3252

[3] Pogaku, N., Prodanovic, M., Green, T.C.: 'Modeling, analysis and testing of autonomous operation of an inverter-based microgrid', *IEEE Trans. Power Electron.*, 2007, **22**, (2), pp. 613–625

[4] Dobson, I., Zhang, J., Green, S.*, et al.*: 'Is strong modal resonance a precursor to power system oscillations?', *IEEE Trans. Circuit Syst. I, Fundam. Theory Appl.*, 2001, **48**, (3), pp. 340–349

[5] Katerei, F., Iravani, M.R., Lehn, P.W.: 'Small-signal dynamic model of a micro-grid including conventional and electronically interfaced distributed resources', *IET Gener. Transm. Distrib.*, 2007, **1**, (3), pp. 369–378

[6] Kroutikova, N., Hernandez-Aramburo, C.A., Green, T.C.: 'State-space model of grid-connected inverters under current control mode', *IET Electr. Power Appl.*, 2007, **1**, (3), pp. 329–338

[7] Krismanto, A.U., Mithulananthan, N., Lee, K.Y.: 'Comprehensive modeling and small signal stability analysis of RES-based microgrid'. 9th IFAC Symp. on Control of Power and Energy Systems (CPES), New Delhi, 2015

[8] Krismanto, A.U., Mithulananthan, N., Krause, O.: 'Microgrid impact on Low frequency oscillation and resonance in power system'. ISGT Asia Pacific 2016, Melbourne, 2016

[9] Dobson, I., Barocio, E.: 'Perturbations of weakly resonant power system electromechanical modes', *IEEE Trans. Power Syst.*, 2005, **20**, (1), pp. 330–337

[10] Beerten, J., D'Arco, S., Suul, J.A.: 'Identification and small-signal analysis of interaction modes in VSC MTDC systems', *IEEE Trans. Power Deliv.*, 2016, **31**, (2), pp. 888–897

[11] Dobson, I.: 'Strong resonance effects in normal form analysis and subsynchronous resonance'. Bulk Power System Dynamic and Control V, Onomichi, Japan, 2001

[12] Krause, P.C., Wasynczuk, O., Sudhoff, S.D.: '*Analysis of electric machinery and drive system 2nd edition*' (Wiley-Interscience, 2002)

[13] Ugalde-Loo, C.E., Ekanayake, J.B., Jenkins, N.: 'State-Space modeling of wind turbine generators for power system studies', *IEEE Trans. Ind. Appl.*, 2013, **48**, pp. 223–232

[14] Erickson, R.W., Maksimovic, D.: '*Fundamental of power electronics second edition*' (Kluwer Academic Publisher, University of Colorado Boulder, Colorado, 2001)

[15] Rahim, N.A., Quaicoe, J.E.: 'Small signal model and analysis of a mulitple feedback control scheme for three phase voltage source UPS inverter'. Proc. of Power Electronics Specialist Conf., Boveno, Italy, 1996

[16] Wu, R., Dewan, S.B., Slemon, G.R.: 'A PWM AC-to-DC converter with fixed switching frequency', *IEEE Trans. Ind. Appl.*, 1990, **26**, (5), pp. 880–885

[17] Wu, R., Dewan, S.B., Slemon, G.R.: 'Analysis of an AC-to-DC voltage source converter using PWM with phase and amplitude control', *IEEE Trans. Ind. Appl.*, 1991, **27**, (2), p. 12

[18] Anaya-Lara, O., Jenkins, N., Ekanayake, J.*, et al.*: '*Wind generation: modelling and control*' (John Wiley & Sons, Ltd, 2009)

[19] Bin, W., Lang, Y., Zargari, N.*, et al.*: '*Power conversion and control of wind energy Systems*' (Wiley, 2011)

[20] Lin, C.m., Vittal, V., Kliemann, W.*, et al.*: 'Investigation of modal interaction and Its effects on control performance in stressed power system using normal form of vector fields', *IEEE Trans. Power Syst.*, 1996, **11**, (2), pp. 781–787

[21] Nomikos, B.M., Vournas, C.D.: 'Modal interaction and PSS design'. IEEE Power Tech Conf., Porto, Portugal, 2001

[22] Kundur, P., Balu, N.J., Lauby, M.G.: '*Power system stability and control*' (McGraw-Hill, New York, NY, USA, 1994)

7 Appendix

See Table 2 overleaf.

Table 2 System parameters

Parameter	Symbol	Value
rated voltage	V_{base}	690 V
parasitic resistance of DC/DC inductor	R_b	1 mΩ
DC/DC inductor	L_b	2 mH
parasitic resistance of DC/DC capacitor	R_{cb}	1 mΩ
DC/DC capacitor	C_b	1000 μF
AC input side inductance of AC/DC	L_{sw}	1 mH
AC input side capacitor of AC/DC	C_{inw}	1000 μF
AC side resistance of AC/DC converter	R_{sdcw}	10 mΩ
DC side capacitor of DC/AC converter	C_{coutw}	1000 μF
DC side inductance of DC/AC inverter	L_{sdcw}	6.43 mH
DC link inductance	L_{link}	0.01 mH
DC link resistance	R_{link}	1 mΩ
DC link capacitance	C_d	6500 μF
low-pass filter inductance	L_{f}	1 mH
low-pass filter capacitance	C_{f}	100 μF
low-pass filter resistance	R_{f}	1 mΩ
coupling inductance	L_c	0.1 mH
coupling resistance	R_c	1 mΩ
load resistance	R_{lo}	0.95 Ω
load inductance	L_{lo}	10 mH
line resistance (buses 1, 2 and 3)	R_{li}	10 mΩ
line inductance (buses 1, 2 and 3)	L_{li}	1 mH